Spectroelectrochemical studies of hole percolation on functionalised nanocrystalline TiO₂ films: a comparison of two different ruthenium complexes†

Xiaoe Li,[a] Mohammad K. Nazeeruddin,[b] Mukundan Thelakkat,[c] Piers R. F. Barnes,[a] Ramón Vilar[a] and James R. Durrant*[a]

We report the application of spectroelectrochemical techniques to compare the hole percolation dynamics of molecular networks of two ruthenium bipyridyl complexes adsorbed onto mesoporous, nanocrystalline TiO₂ films. The percolation dynamics of the ruthenium complex *cis*-di(thiocyanato)(2,2′-bipyridyl-4,4′-dicarboxylic acid)-(2,2′-bipyridyl-4,4′-tridecyl) ruthenium(II), N621, is compared with those observed for an analogous dye with an additional tri-phenyl amine (TPA) donor moiety, *cis*-di(thiocyanato)(2,2′-bipyridyl-4,4′-dicarboxylic acid)-(2,2′-bipyridyl-4,4′-bis(vinyltriphenylamine)) ruthenium(II), HW456. The *in situ* oxidation of these ruthenium complexes adsorbed to the TiO₂ films is monitored by cyclic voltammetry and voltabsorptometry, whilst the dynamics of hole (cation) percolation between adsorbed ruthenium complexes is monitored by potentiometric spectroelectrochemistry and chronoabsorptometry. The hole diffusion coefficient, D_{eff}, is shown to be dependent on the dye loading on the nanocrystalline TiO₂ film, with a threshold observed at ∼60% monolayer surface coverage for both dyes. The hole diffusion coefficient of HW456 is estimated to be 2.6×10^{-8} cm²/s, 20-fold higher than that obtained for the control N621, attributed to stronger electronic coupling between the TPA moieties of HW456 accelerating the hole percolation dynamics. The presence of mercuric ions, previously shown to bind to the thiocyanates of analogous ruthenium complexes, resulted in a quenching of the hole percolation for N621/TiO₂ films and an enhancement for HW456/TiO₂ films. These results strongly suggest that the hole percolation pathway is along the overlapped neighbouring -NCS groups for the N621 molecules, whereas in HW456 molecules cation percolation proceeds between intermolecular TPA ligands. These results are discussed in the context of their relevance to the process of dye regeneration in dye sensitised solar cells, and to the molecular wiring of wide bandgap inorganic materials for battery and sensing applications.

Introduction

The functionalisation of nanocrystalline mesoporous metal oxide films with molecular and biomolecular materials has been widely studied over the past two decades for device applications ranging from nanostructured optoelectronic devices (such as solar cells or light emitting diodes) to chemical and biochemical sensors.[1–5] In particular, it has recently been shown that the adsorption of molecular redox active species to such films can result in efficient lateral hole transport across the internal surface of the films. Such charge percolation is currently under investigation to enable the molecular wiring of otherwise insulating inorganic films for battery and transistor applications.[6–11] Studies of such charge percolation to date have focused upon ruthenium dyes, fullerene derivatives and aromatic amines. Bonhôte, *et al.*[8] studied a phosphonated triarylamine anchored to nanocrystalline TiO₂ films, demonstrating hole transport across the adsorbed amine layer, with a percolation threshold of ∼50% of a full monolayer coverage. Meyer, *et al.*[9] extended such studies to osmium bipyridyl complexes adsorbed onto TiO₂ films. Papageorgiou, *et al.*[10] observed the lateral electron transport across a monolayer of derivatised fullerenes bound to a nanocrystalline ZrO₂ film, whilst other studies have focused on ruthenium bipyridyl dyes.[7]

The kinetics of the hole percolation process are critical to potential device applications. These kinetics are of possible importance to the function of dye sensitised nanocrystalline solar cells (DSSCs), where such percolation processes may result in the transport of dye cations across the sensitised TiO₂ surface prior to regeneration by the redox electrolyte. However, to date, the correlation between molecular structure and the dynamics of hole percolation has only received limited attention. Wang *et al.* have proposed that the presence of thiocyanate ligands in ruthenium bipridyl dyes aids the molecular packing of the dye layer and thus the kinetics of

[a] *Department of Chemistry, Imperial College London, London SW7 2AZ, UK. E-mail: j.durrant@imperial.ac.uk; Fax: +44(0)2075945621; Tel: +44(0)2075945321*
[b] *Laboratory for Photonics and Interfaces, Institute of Molecular and Biological Chemistry, School of Basic Sciences, Swiss Federal Institute of Technology, CH-1015 Lausanne, Switzerland*
[c] *Applied Functional Polymers, University of Bayreuth, Bayreuth, 95440, Germany*
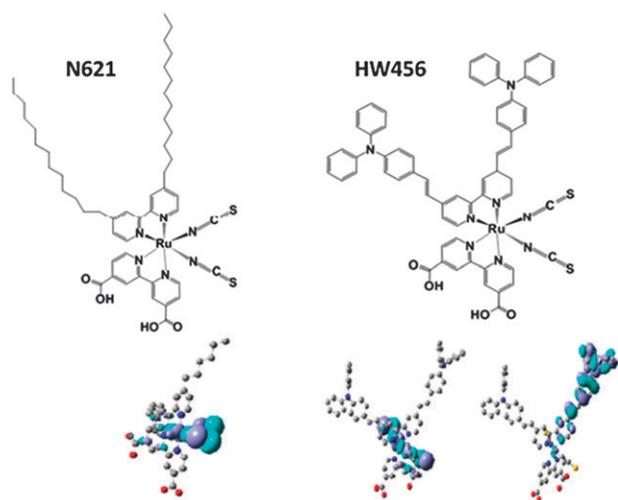
Scheme 1 Molecular structures of N621 and HW456, and graphical representations of the dye cation HOMO orbitals as determined from DFT calculations (bottom from left to right: N621 neutral, HW456 neutral and HW456 cation).

hole percolation.[7] In this paper we compare the percolation dynamics for two ruthenium bi-pyridyl complexes with and without the inclusion of a tri-phenyl amine (TPA) electron donating group. We demonstrate that the inclusion of the TPA group results in a twenty fold enhancement of the diffusion constant for hole percolation, and discuss the implications of this observation for technological applications.

Donor–acceptor dyes have been shown to be attractive sensitiser dyes for DSSCs, due both to their high molar extinction coefficients and their potential to generate remarkably long-lived photoinduced charge separation at the dye/metal oxide interface.[12,13] By introducing a π-electron donor, such as TPA, into the dye structure, the positive charge or 'hole' is shifted on to this moiety, potentially increasing the distance between the dye cation and the metal oxide surface, and thus retarding the interfacial charge recombination dynamics. One such dye is HW456 (cis-di(thiocyanato)(2,2′-bipyridyl-4,4′-dicarboxylic acid)-(2,2′-bipyridyl-4,4′-bis(vinyltriphenyl-amine) ruthenium(II), (Scheme 1) which has shown good device performance in both solid state and liquid electrolyte DSSCs.[14,15] In this study, the performance of HW456 is compared with that of a control dye, N621 (cis-di(thiocyanato)-(2,2′-bipyridyl-4,4′-dicatboxylic acid)-(2,2′-bipyridyl-4,4′-tri-decyl) ruthenium(II)), where the TPA electron donating groups are replaced by alkyl chains. Both the HW456 and N621 dyes adsorb strongly onto nanocrystalline TiO₂ films dye via their carboxylic acid groups. In this paper, we focus on the impact of the different donor substituents on the dynamics of hole percolation when these dyes are adsorbed to nanocrystalline TiO₂ films.

The anatase phase of TiO₂ considered in this work is a wide band gap (3.2 eV) n-type semiconductor and is thus effectively insulating where its Fermi level is within the bandgap between the TiO₂ conduction and valence band edges (corresponding to approximately −0.1 V and +3.1 V versus NHE at pH 1, respectively[16]). The oxidation potentials of the two ruthenium(II) dyes considered in this paper both lie in the centre of this

bandgap. Consequently, for the application of electrical potentials close to the dyes' oxidation potentials, the TiO₂ film functions only as an insulating supporting material. Functionalisation of such films with these dyes thus allows us to study the lateral percolation of holes across the adsorbed molecular film. The fabrication of such films on conducting substrates such as FTO allows the application of positive potentials sufficient to oxidise dye molecules adjacent to the FTO substrate. The subsequent percolation of dye cations (or 'holes') via two-dimensional hopping across the molecular network can be observed when the dye surface coverage exceeds the percolation threshold.

Spectroelectrochemistry, which combines electrochemical perturbation of an optically transparent electrode with simultaneous optical absorption monitoring, has been successfully applied to provide remarkably detailed information about the mechanism of both homogeneous and heterogeneous electrochemical reactions.[3,17,18] These techniques allow the species of interest to be optically monitored directly. One such technique is cyclic voltabsorptometry (CVA), measurement of the optical absorbance as a function of cycling potential, which can be conducted simultaneously with cyclic voltammetry. The differentiated cyclic voltabsorptometry signal (DCVA, dA/dE or dA/dt, the derivative of optical absorption A with respect to the potential E (or time t) at a fixed wavelength λ), can show a similar shape to conventional CV (since dA/dt is proportional to electrode current) but with a much cleaner signal.

DCVA has been employed to investigate the redox processes of proteins adsorbed to nanocrystalline metal oxide films,[3] rutin[19] and conducting polymer films such as polyaniline,[20,21] poly(3,4-ethylenedioxythiophene)[22] and poly(3,4-dimethoxy-thiophene),[23] which is insensitive both to film charging and faradic currents. In addition, potential step absorption spectro-electrochemistry techniques, such as chronoabsorptometry, has been intensively utilized to study lateral electron/hole transport in electroactive species and has proven to be a useful technique for the determination of heterogeneous electron transfer kinetic parameters, such as the reaction rate and diffusion coefficients.[7,8]

In this paper, the hole percolation dynamics of both N621/TiO₂ and HW456/TiO₂ have been investigated. Spectro-electrochemical techniques have been employed to monitor the electroactivity and hole percolation. The dependence of these percolation dynamics upon the presence mercuric ions is used to provide further insight into the different mechanisms of hole percolation between these two molecules.

Experimental details

All the solvents and chemicals, unless otherwise stated, were obtained from Sigma-Aldrich or their subsidiaries and were used without further purification. All experiments were performed at room temperature.

The fabrication of nanocrystalline, mesoporous TiO₂ films involves the preparation of a TiO₂ paste by sol-gel processing followed by hydrothermal treatment.[24] Mesoporous nano-crystalline TiO₂ films comprising 15 nm sized anatase TiO₂ particles were prepared as follows: 40 ml of titanium iso-propoxide were mixed with 9.1 g of glacial acetic acid under

a nitrogen atmosphere and stirred for 10 minutes. The mixture was then poured into a conical flask containing 240 ml of 0.1 M nitric acid solution at room temperature and it was subsequently stirred at 80 °C for 8 hours. The TiO_2 colloid was first filtered using a 0.45 μm syringe filter and then autoclaved at 220 °C for 12 hours. The colloid was re-dispersed with a 2 min cycle burst from a LDU Soniprobe horn. The solution was then concentrated to 12.5% (in TiO_2 weight) on a rotary evaporator at 45–50 °C. Carbowax 20 000 (50% of TiO_2 by weight) was added and the resulting paste was stirred slowly overnight prior to film deposition to ensure film homogeneity and that no air bubbles were trapped. The paste was spread on the FTO substrates using a glass rod with one layer of 3 M adhesive tapes used as spacer. After drying in air, the film was sintered at 450 °C for 30 minutes in a furnace. The resulting film thickness was of *ca.* 4 μm, measured by using an Alpha-step 200 surface profilometer (Tencor Instruments, USA).

Dye solutions were prepared in the concentration range of $0.02–2 \times 10^{-4}$ M in 1 : 1 (v/v) acetonitrile and *tert*-butanol solution for N621 and in chloroform for HW456; the TiO_2 films were dipped into the dye solutions for two days, with the final dye loading depending upon solution concentration. UV-Vis absorption spectra of dye sensitised TiO_2 films were monitored at room temperature using Thermo Genesys 10 UV-Vis Spectrophotometer and the optical density was used to calculate the dye loading.

Electrochemical and *in situ* optical spectroelectrochemical experiments were carried out in a three-electrode spectro-electrochemical single-compartment-cell configuration, which was connected to an Autolab PGStat 12 potentiostat. The cell comprised 2.5 mL of electrolyte-tetrabutylammonium perchlorate (TBAP) in acetonitrile predried using Molecular Sieves 5H, sandwiched between two quartz windows, employing a working electrode (dye sensitised TiO_2 film), an auxiliary electrode (a platinum mesh flag) and a reference electrode (quasi-reference electrode (QRE) platinum wire). The potential of the platinum wire QRE was found to be −0.4 V *versus* the ferrocene/ferrocenium couple. All potentials are stated *versus* ferrocene/ferrocenium couple.

The above three-electrode cell was incorporated in the sample compartment of a Shimadzu UV-1601 spectrophotometer and the absorption changes were monitored as a function of applied step or sweep potential. Cyclic voltammetry (CV, measurement of the current as a function of the applied sweep potential) and cyclic voltabsorptometry (CVA) were conducted simultaneously. CVs were obtained at a scan rate of 100 mV s⁻¹. Chronoabsorptometry measurements recorded the corresponding optical spectra (wavelength 300–900 nm) as a function of the applied step potential (−0.4 V to 0.6 V and 0.8 V *vs.* Fc/Fc^+ for N621 and HW456 respectively). The apparent diffusion coefficients of hole hopping through neighbouring adsorbed dye molecules by percolation were measured at different dye loadings using chronoabsorptometry measurements employing classical chronocoulometric methodologies.[25]

Results

As discussed above, lateral hole percolation across adjacent molecules adsorbed onto a nanocrystalline metal oxide film

has been studied using spectroelectrochemical techniques, in order to obtain the percolation threshold and the hole diffusion coefficient. We show that the kinetics of the hole percolation is affected by the HOMO position, molecular structure and orientation.

DFT calculations of N621 and HW456 molecules

Herein a hole is considered to be an unfilled HOMO orbital. This is formed after the molecule is oxidised to form a dye cation. Density functional theory (DFT) calculations of the dyes' neutral and cation HOMO orbitals were performed by employing B3LYP/LANDZ parameters using Gaussian. The calculations confirmed HOMO orbitals are localised upon the NCS groups for neutral (first oxidation state) HW456 molecules and spread over the phenyl amine moieties (TPA) for HW456 cations (second oxidation state). For N621, the HOMO (cation) orbitals are essentially ruthenium t_{2g} character with sizable contribution coming from the NCS ligand orbitals (Scheme 1). This implies that the first oxidation in both complexes is still dominated by ruthenium t_{2g} character. In comparison, the second oxidation state in HW456 (the HOMO of the cation) is primarily located on the TPA group.

Steady state spectroscopy and dye loading

The optical transparency of nanocrystalline TiO_2 films, which shows negligible absorbance in the visible region, makes it feasible for spectroelectrochemical measurements of absorbed molecules. Moreover, the insulating properties of nanocrystalline TiO_2 films in the examined potential range (0.4 V to +0.8 V *vs.* Fc/Fc^+) provides a background free platform for monitoring the oxidation reactions of adsorbed N621 and HW456 dye molecules. Therefore, the redox processes and the hole percolation kinetics of both N621 and HW456 dye molecules can be investigated using the N621/TiO_2 and HW456/TiO_2 films as working electrodes under an applied potential step or a positve bias sweep.

The steady state absorption spectra of N621/TiO_2 and HW456/TiO_2 films are shown in Fig. 1. A control TiO_2 film spectrum is shown for comparison. The absorption bands at 530 nm for N621 and at 425 nm and 540 nm for HW456 correspond to metal-to-ligand charge-transfer (MLCT) transitions.[20,26]

The surface loading of dye molecules on mesoporous nanocrystalline TiO_2 films, the number of dye molecules in
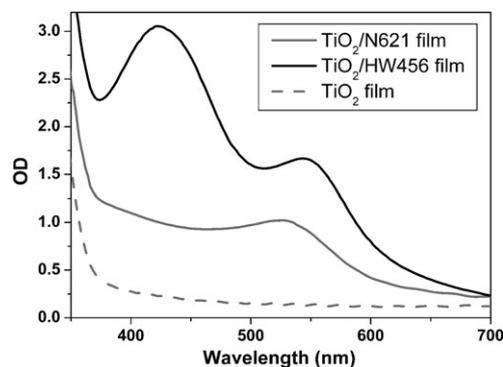
Fig. 1 UV-Vis spectrum of N621/TiO_2 film (grey), HW456/TiO_2 film (black) and control TiO_2 film (light grey, dash).

moles per unit projected area of the TiO$_2$ films (μmol/m^2), (n_d = OD/($\varepsilon \times 10^3$)), was calculated by Beer-Lambert law employing the molar extinction coefficient of 7830 M^{-1} cm^{-1} at wavelength 530 nm for N621 and 24 600 M^{-1} cm^{-1} at 540 nm for HW456, respectively.[12,27] The equilibrium dye loading for mesoporous nanocrystalline TiO$_2$ films at different dye concentrations were fitted by the Langmuir adsorption isotherm (eqn (1)).[28]

$$\frac{\Gamma}{{}^S\Gamma} = \frac{K_f * C}{1 + K_f * C} = \frac{C}{\left(C + \frac{1}{K_f}\right)} \tag{1}$$

where Γ is the number of surface loaded dye molecules (moles per unit surface area of TiO$_2$ films, mol m^{-2}) and ${}^s\Gamma$ is the number at full monolayer surface coverage; C is the concentration of the dye solution and K_f is the binding constant, defined as the ratio of adsorption and desorption rates for dye molecules on the surface of TiO$_2$ films. Γ is related to n_d by equation $\Gamma = n_d/\eta$, where η is defined as the films roughness factor, which was determined by BET analyses of film surface area (in this case, η is 450).[29] At a full monolayer dye coverage, ${}^s\Gamma = 3.42 \pm 0.02$ and 1.64 ± 0.02 μmol/m^2 for N621 and HW456, corresponding to saturated dye coverages of 2.0×10^{18} and 9.8×10^{17} molecules per m^2 TiO$_2$ surface for N621 and HW456 respectively (with binding constants $K_f = 12.2 \pm 3.4$ and 8.1 ± 3.5 mM^{-1} for N621 and HW456 respectively). From these data, the estimated surface area one dye molecule occupies, $S_{mol} = 1/({}^s\Gamma \times N_a)$, (where N_a is the Avogadro number), is 0.5 and 1 nm^2 for N621 and HW456 respectively. This is in reasonable agreement with the molecular dimensions determined from modelling studies. Consequently, the lower packing density of HW456 molecules adsorbed on mesoporous nanocrystalline TiO$_2$ films implies a greater distance between adjacent HW456 molecular cores than in the case of N621.

Potentiometric spectroelectrochemistry

The change of the UV/Vis absorption spectra for N621/TiO$_2$ and HW456/TiO$_2$ films before and after the application of positive oxidation potentials is shown in Fig. 2. These changes in absorption spectra are assigned to dye oxidation. The applied electrode potential is stepped from a potential where no current flows (e.g. -0.4 V vs. Fc/Fc$^+$) to one at which dye cations are formed ($+0.6$ V vs. Fc/Fc$^+$ for N621 or $+0.8$ V vs. Fc/Fc$^+$ for HW456). The absorption spectra of the oxidised dye were taken after ca. 4 minutes, allowing time for saturation of the dye oxidation processes (see below). The spectra are characterised by loss of the MLCT ground state absorption bands at 530 and 540 nm, and the appearance of cation absorption bands at 770 and 750 nm, for N621 and HW456 respectively. The magnitude of these absorption changes are indicative of extensive ($>50\%$) oxidation of the adsorbed dye molecules in both cases. The absorption in the near IR region (770 nm) is due to transitions from ligand orbitals to the d^5 ruthenium cation (LMCT). The slight blue shift of the near IR band in the HW456 (750 nm) as compared to that of N621 is assigned to de-stabilization of ruthenium orbitals caused by the donor strength of TPA group. The enhanced optical density of the near IR band in HW456 indicates that in
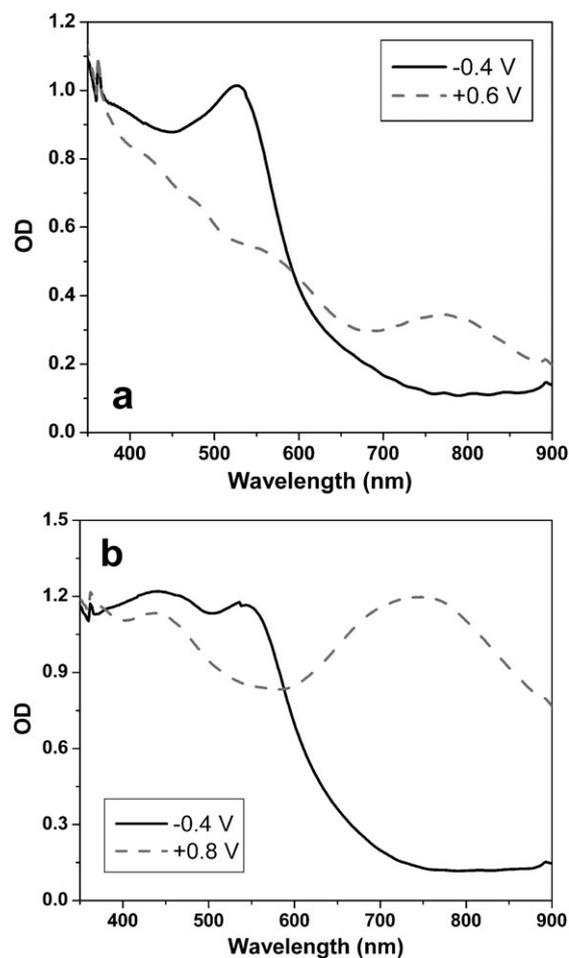
Fig. 2 UV-Vis spectra of neutral (solid) and oxidized (dashed) N621(a) and HW456(b) adsorbed on mesoporous TiO$_2$ electrodes measured ca. 4 minutes after the application of the potentials indicated. The electrolyte is 0.1 M TBAP in acetonitrile.

addition to the NCS ligands, the TPA group is also involved in these LMCT transitions.[15] Similar results obtained with the N621/ZrO$_2$ films confirm that metal oxide films are insulating suppoting materials in the potential range examined, and thus electrons in TiO$_2$ conduction band have no effect on the dye oxidation.

Following prolonged oxidation (more than 20 minutes), both sensitiser dyes showed absorption changes that were quasi-reversible. This is consistent with the vulnerability to decomposition shown by similar NCS dyes containing ruthenium reported previously[30] where oxidative degradation forms cis-RuL$_2$(CN)$_2$ (L = 2,2$'$-bipyridine-4,4$'$-bisphosphonic acid) indicated by an absorption peak at 450 nm.[31] We compared the rate of dye degradation ($k_{degradation}$, estimated by normalising the differentiated ΔOD with respect to time, eqn (2)) with the rate of hole tranport ($k_{transport}$, estimated by eqn (3), where D_{app} is the hole diffusion coefficient, d is the film thickness):[32]

$$k_{degradation} = -\frac{1}{\Delta OD}\frac{d\Delta OD}{dt} \tag{2}$$

$$k_{transport} = \frac{\pi^2 D_{app}}{4d^2} \tag{3}$$

It was found that $k_{transport} \sim 0.40$ s^{-1} which was much greater than the maximum $k_{degradation} \sim 9.8 \times 10^{-3}$ s^{-1} for HW456 dye (Fig. S1†). This implies that the degradation of dye cations is not fast enough to significantly influence our conlusions on percolation dynamics. To analyse percolation dynamics more precisely, transient electrochemical measurements were used on a time scale which avoids dye degradation.

Cyclic voltammetry

Voltammetric and *in situ* spectroelectrochemical measurements were conducted in a three-electrode cell. The resulting current cyclic voltammetry (CV), and cyclic voltabsorptometry (CVA) of N621/TiO$_2$ films are displayed as a function of applied sweep potential in Fig. 3.

The CV signal monitors the current flow corresponding to the change in film redox state. By contrast, the CVA signal, monitoring the film's optical density at the dye cation absorption maxima, tracks the total cation population. Comparison of the CVA and CV data is thus facilitated by differentiation of the CVA data, yielding the DCVA data shown in Fig. 3c. As the dye cation absorption peak (750 nm) is chosen to monitor the redox change of N621 in the optical measurement (CVA), DCVA is insensitive both to film charging and faradaic currents. It is apparent that the cyclic voltammetry data is well matched by the DCVA data, indicating that the effect of capacitive current is relatively negligible and confirming the CV data is due to the dye itself.

In Fig. 3, a quasi-reversible one-electron transfer process is observable in both the CV and DCVA traces for the N621/TiO$_2$ film, with a mid-point potential $E_{1/2}$ at 0.25 V vs. Fc/Fc$^+$, which is in agreement with free dye in solution (Fig. S2 in the Supporting Information†) and previous observations on dye sensitised films.[27] The increase and then decrease of absorbance in the CVA, correspond to the Ru(II)-NCS to Ru(III)-NCS oxidation and the Ru(III)-NCS to Ru(II)-NCS reduction, respectively. The trend of DCVA is in good correlation with the nearly reversible, well defined anodic and
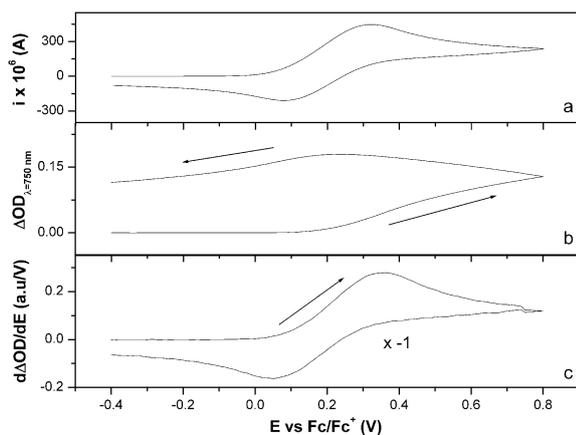
Fig. 3 Spectroelectrochemical characterisation CV (a), CVA (b), and DCVA (c) of N621 on nanocrystalline TiO$_2$ film at a scan rate of 100 mV/s. Arrows show the scan directions. In order to make it readily comparable to CV data, the oxidation process in the DCVA data were multiplied by −1. All experiments were measured in non-aqueous solution (0.1 M TBAP in acetonitrile).

cathodic peak currents in the CV results (Fig. 3a). However, the CVA and DCVA results of HW456/TiO$_2$ films are more complex, typically exhibiting two oxidation waves with mid-point potentials at 0 V and 0.5 V vs. Fc/Fc$^+$, as shown in Fig. S3 in the Supporting Information.† A more detailed electrochemical study of HW456 is reported elsewhere.[12] For the purposes of this discussion, it is enough to note that +0.8 V is sufficient to oxidise both dye molecules. To determine the charge passed through the dye/TiO$_2$ films and thus the fraction of oxidized dye molecules, the current vs. time curves from the CV data (Fig. 3a and S3) are integrated. The calculation shows that one-third of N621 and almost all HW456 molecules have been oxidised within 12 and 15 second for TiO$_2$ films with full surface dye coverage, respectively. As we discuss below, this is consistent with the faster hole transport in HW456/TiO$_2$ films relative to N621/TiO$_2$ films.

Hole percolation

Classical percolation behaviour is characterised by a sharp concentration threshold below which percolation and consequently charge conduction cannot occur due to a lack of continuously connected clusters of conducting sites (in this case dye molecules).[33] In the dye functionalised TiO$_2$ films studied herein, previous studies have shown that when the surface coverage of dye molecules (dye loading) exceeds a threshold concentration, the molecules rapidly switch from disconnected non-conducting 'islands' to a connected conducting network, through which charge can be transported in the film.[8] CV and chronoabsorptometry data of a series of dye sensitized TiO$_2$ films with varying dye loading were therefore measured to obtain the hole diffusion coefficient and the percolation threshold.

The kinetics of dye cation formation were determined from chronoabsorptometry measurements (*i.e.* monitoring of optical absorption change induced by a step change in electrical potential applied to the film) measured at the dye cation absorption maxima (770 nm and 750 nm for N621 and HW456 respectively). Typical data measured at full monolayer dye coverage is shown in Fig. 4a. It is apparent that the kinetics of dye cation formation is significantly faster for HW456 compared to N621. For HW456, the optical response exhibits a half time of ~ 3 s, and saturates at ~ 20 s. By contrast, for N621, the signal did not saturate in the time scale plotted, and exhibited an estimated lifetime of > 20 s. Quantitatively, the experimental data were fitted using a modified version of the Cottrel equation[25] given by eqn (4). This relationship gives a good approximation to the exact solution for the diffusion of holes through a thin layer for times where $t < d^2/(4D_{app})$ (see Appendix for details).

$$\Delta OD(\lambda, t) = \frac{2\Delta OD_f}{d} \sqrt{\frac{D_{app}t}{\pi}} \qquad (4)$$

Here ΔOD is the absorbance change at time t and ΔOD_f is the total absorbance change; D_{app} is the apparent charge-transfer diffusion coefficient in cm^2/s; the film thickness d is 4 μm in this study. Typical fits are shown in Fig. 4b, showing reasonable agreement with the experimental data, yielding value for
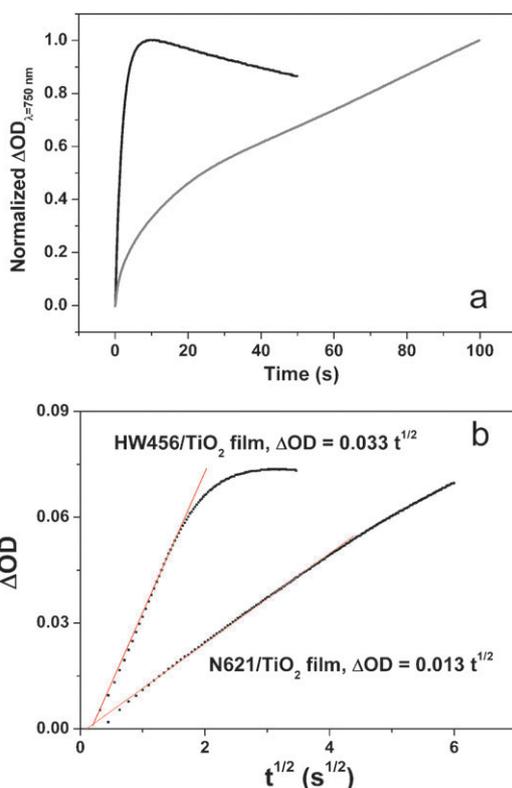
Fig. 4 (a) Formation time of dye cations at a potential step of $+0.3$ V or $+0.6$ V $vs.$ Fc/Fc$^+$ for HW456 (black) and N621 (grey) and (b) ΔOD plotted as a function of $t^{1/2}$ and the fitting of the data using eqn (4) (data-points, fit-solid line).

D_{app} of 2.6×10^{-8} and 1.2×10^{-9} cm^2/s for HW456 and N621, respectively.

Measurements similar to those shown in Fig. 3 and 4 were made for films with different dye loading. The hole diffusion coefficient was found to be dependent on the dye loading on the nanocrystalline TiO$_2$ films. The dependence of the anodic current and diffusion coefficient on dye surface coverage are shown in Fig. 5a (N621) and 5b (HW456). The apparent diffusion coefficient D_{app} was determined at different dye surface coverages ($= \Gamma/^s\Gamma$) from chronoabsorptometry data fitted by eqn (4), where ΔOD_f was determined at sufficienctly long time and the gradient was found from the linear region of the slope where $t < d^2/(4D_{app})$.

The hole diffusion coefficient D_{app} of both the N621/TiO$_2$ and HW456/TiO$_2$ films increases dramatically at $\Gamma/^s\Gamma > 60\%$. For N621/TiO$_2$ the D_{app} values are also compared with an alternative estimate of D_{app} determined by analysing the maximum anodic current from the CV data using eqn (5) (the data are plotted in Fig. 5a).[25] It can be seen that at full dye loading, D_{app} from CV is 4.5×10^{-9} cm^2/s, somewhat larger than the value estimated from chronoabsorptometry data but with a similar magnitude. The difference may be related to the irreversible formation of an oxidation species (for example [Ru(LL)$_2$(CN)$_2$])[31] which partially cancels the ΔOD signal from the cation.

$$j_p = (2.69 \times 10^5)z^{\frac{3}{2}}D_{app}^{\frac{1}{2}}C_0v^{\frac{1}{2}} \quad (5)$$
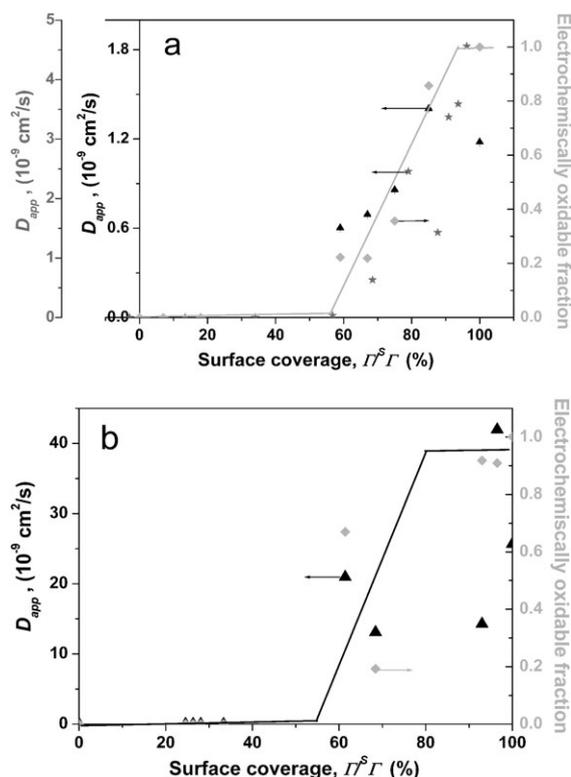
Fig. 5 The D_{app} (grey stars, from fits to j_p $vs.$ $v^{1/2}$ with eqn (5), far left Y axis), D_{app} (black triangles, from chronoabsorptiometry data fitted with eqn (4), left Y axis) and electrochemically oxidizable fraction (grey diamonds, right Y axis) of **(a)** N621/TiO$_2$ and **(b)** HW456/TiO$_2$ films, following a potential step from -0.4 V to $+0.6$ V ($vs.$ Fc/Fc$^+$) for N621 and 0 V to 0.7 V ($vs.$ Fc/Fc$^+$) for HW456 as a function of the dye surface coverage. The electrolyte is 0.1 M TBAP in acetonitrile for both CV and chronoabsorptometry measurements. All experiments were measured at a scan rate of 100 mV/s. The lines across the experimental dots (grey diamonds) are plotted to mark the percolation threshold.

Here j_p is the peak anodic current density in amperes/cm^2, $z = 1$ is the number of electrons consumed in the electrode reaction (in this case, dye oxidation/reduction), D_{app} is the hole diffusion coefficient in cm^2/s, C_0 is the dye concentration in the mesoporous TiO$_2$ films in mol/cm^3, and v is the scan rate in V/s.

The similarity of the onset and variation of D_{app} determined by these different methods (chronoabsorptometry and CV) suggests that a rough approximation of the percolation controlled hole diffusion coefficient has been found, in line with the previous discussions.[7,8] The similarity of the percolation threshold demonstrates that the current flow is due to the hole transport across the surface-coated TiO$_2$ nanoparticles. Below this threshold, there are not enough dye molecules to create a lateral percolation pathway on TiO$_2$ surface.

Also plotted in Fig. 5 (grey diamonds, right Y axis) is the electrochemical oxidisable fraction of dye ($= (\Delta OD_f/n_d)/(\Delta OD_f/n_d)_{max}$, where n_d is the number of dyes molecules in moles per unit TiO$_2$ films projected area (μmol/m^2)) as a function of surface coverage. This shows a similar percolation threshold ($\Gamma/^s\Gamma \sim 60\%$) for both dyes and indicates that a progressively larger proportion of the molecules on the surface

can be oxidised as the surface coverage increases. This is expected as the fraction of molecules belonging to percolating clusters connected to the substrate increases.

Previously studies have demonstrated a strong interaction between the sulfur p-orbitals of -NCS groups in ruthenium complexes such as N719[2] and Z907[7] and mercuric ions, apparent for example as a colour change from red to yellow of N719/TiO$_2$ films in the presence of mercuric ions.[7,34] The quenching of anodic current of N621/TiO$_2$ electrode by addition of mercuric ions is observed, as shown in Fig. S4a,† in agreement with previous observation.[27] However, for the HW456/TiO$_2$ electrode, which has shown a high diffusion coefficient for lateral hole-transfer percolation, the presence of mercuric ions increases the anodic current of HW456 (Fig. S4b†). This opposite effect of mercuric ions implies different hole percolation mechanisms for the two Ru-complexes, as we discuss below.

Discussion

We consider first the process of hole pecolation through hole hopping between the adjacent molecules adsorbed on the nano-crystalline TiO$_2$ films. This is only observed on a macroscopic (film) scale when the dye surface coverage is above the percolation threshold, where dye molecules have sufficient conductivity to create a conducting pathway for charge transport. During the oxidation of the dye molecules following an applied positive potential, holes are injected into the film *via* the attached molecules from the FTO substrate and across the dye molecules anchored to the TiO$_2$ film surface, as shown in Scheme 2.

The single bi-(carboxypyridine) (dcbpy) group of both dyes are responsible for anchoring the dye to the TiO$_2$ substrate and result in significant flexibility in binding orientation.[35] This flexibility is likely to be important in enabling the sensitiser dyes to orientate on the TiO$_2$ surface so as to favour intermolecular electronic coupling, and thus hole transfer. This has been discussed previously for the Z907 sensitiser dye,[35] analogous to N621 (C13) but with a shorter alkyl chain (C9), where molecular modelling calculations suggested monolayer dye binding would result in significant electronic coupling of the NCS groups between molecules. In contrast, for HW456, the lower dye density at monolayer coverage can be expected to reduce NCS group intermolecular interactions, with the primary interactions being between the larger TPA groups.
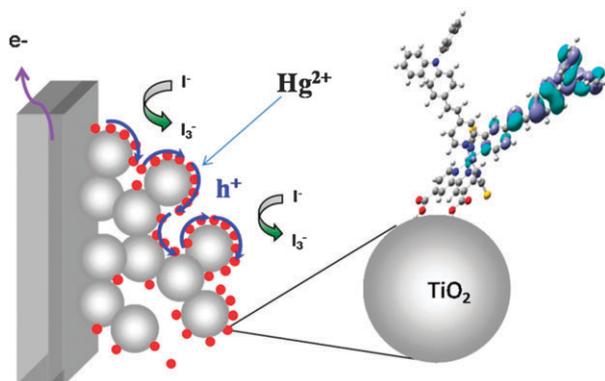
Scheme 2 Schematic model showing the lateral hole transfer percolation along with the mercury interaction.

The hole percolation dynamics are 20-fold faster for donor–acceptor dye HW456 than its N621 analogue without the triphenyl amine (TPA) electron donating moieties, with an apparent hole diffusion coefficient of 2.6×10^{-8} cm^2/s compared to 1.2×10^{-9} cm^2/s at a full monolayer dye surface coverage. This difference in apparent diffusion coefficients is attributed to the presence of the TPA group in HW456 molecules as triphenyl-amines (TPAs) are well known to be good hole transport materials in, for example, solid-state DSSCs.[12,14]

The binding of mercuric ions to both dyes is thought to be primarily due to the NCS groups, forming an NCS-Hg complex.[2,27,32] For N621, this prevents the NCS groups from participating in the intermolecular hole exchange between adjacent dye molecules. This suppresses the hole percolation within the molecule network, which is in agreement with the previous studies of Z907 dye molecules.[7] In contrast, for HW456, the observed increase in hole percolation in the presence of mercuric ions is consistent with hole percolation for this dye being primarily mediated by the TPA groups. We thus conclude that the hole percolation pathway is along the overlapped neighbouring NCS groups for the N621 functionalised films, whereas for the HW456 functionalised films hole percolation is *via* the overlapped intermolecular TPA ligands. The fast hole percolation of HW456 (short transport time ∼5 s) has potential interest for a range of technological applications, such as the molecular wiring of otherwise insulating inorganic films for molecular nanotransistors applications, although we note such applications will probably require the omission of NCS moeities to avoid instability limitations of the dye cation.

We turn now to the relevance of these results to Dye-Sensitised Solar Cell. In DSSCs, the dye cation can undergo two reactions: one is regeneration, in which D$^+$ is reduced by iodide in the electrolyte and the other is the recombination of the D$^+$ with electrons in the TiO$_2$ conduction band. Dye cation (or hole) percolation across the surface of the TiO$_2$ film, has not previously been considered as a significant issue for device function. However, this hole percolation may change dye cation regeneration and recombination dynamics. It could in principle favour device function, for example by enabling dye cations generated in small pores in the TiO$_2$ network, where iodide may have limited access, to move to nearby dyes with better iodide accessibility. Similarly, in solid-state OMeTAD (hole-transport material, HTM) cells, dye cations could be transported between dye molecules in unfilled pores with no HTM to dye molecules in contact with the spiro-OMeTAD. On the other hand, hole percolation could potentially decrease device efficiency either by facilating recombination with trapped TiO$_2$ electrons or by resulting in cation trapping on surface impurities. Therefore, to understand the influence of hole percolation on DSSC's device performance we can make a rough estimation of the relative dynamics of dye regeneration[35] and hole percolation.

The dye cation/hole percolation (or 'diffusion') length in cell can be obtained from the chronoabsorptometry measurements reported herein, coupled with dye cation lifetime kinetics determined by transient absorption spectroscopy (TAS). It can be estimated by eqn (6) as shown in Table 1.

$$L = \sqrt{D_{\mathrm{app}}\tau} \qquad (6)$$

Table 1 Comparison of hole percolation to dye cation regeneration

Film	N621/TiO$_2$	HW456/TiO$_2$
D_{app} (cm^2/s)	1.2×10^{-9}	2.6×10^{-8}
Surface area per dye S_{mol} (nm^2/dye)	0.5	1
Dye cation regeneration time τ (μs)^a	10	25
Hole diffusion length L (nm)	1	8
Numbers of dye molecules in the area πL^2 (nm^2)	6	200

^{a} Regeneration time for dye cation by TAS was determined elsewhere.[15,36]

where L is the hole diffusion length, D_{app} is the hole apparent diffusion coefficient, and τ is the dye cation lifetime, *i.e.* the oxidised dye regeneration time by the electrolyte.

Although dye HW456 shows a slow regneration dynamics compared to N621 dye,[15,36] the hole diffusion coefficient is ~20 times bigger. As a result, the hole diffusion lengths are 1 and 8 nm for N621 and HW456 molecules in DSSCs. This implies that the hole diffusion length of HW456 is about half of a TiO$_2$ particle's diameter (~15 nm), and thus HW456 cations located in a pore which is not well connected to the electrolyte are more likely to reach the redox couple or HTM and be regenerated than N621 cations. In addition, the number of dye molecules within a 'diffusion area', *e.g.* the dye cation or hole percolation area, πL^2, can be estimated to be 6 and 200 nm^2 for dye N621 and HW456 respectively. This diffusion area represents the surface which the dye cation/hole can percolate across the surface-coated TiO$_2$ nanoparticles before regeneration by iodide or the HTM. In this regard, we note that an analogous dye to HW456 has been shown to yield superior performance to N621 in solid state DSSCs employing the HTM spiro-OMeTAD.[12,14] On the other hand, we also note that a higher diffusion area may also facilitate recombination with electrons or hole trapping/recombination at surface impurities. As such, further studies could investigate the effect of hole percolation in DSSCs by measuring the dye regeneration and recombination processes at different dye surface coverages.

Conclusions

The donor–acceptor dye HW456 adsorbed on the nanocrystalline TiO$_2$ film exhibits faster hole percolation due to shifting of HOMO orbitals of ruthenium dye molecules from -NCS ligands to the electron donor group-TPA ligands, compared to the charge transfer dye N621. However, this shift of HOMO orbital location does not stabilise the -NCS groups while dye molecule is oxidized. Further work is underway to find more stable, faster hole percolation donor–acceptor dyes to enable the dye/TiO$_2$ films in applications of the molecular wiring, percolation batteries and molecular nanotransistors.

Appendix

Derivation of the relationship between diffusion coefficient and chronoabsorbtometry

The apparent diffusion coefficients (D_{app}) for hole hopping due to percolation through neighbouring adsorbed dye molecules were measured at different surface coverages of

dye molecules using chronoabsorptometry. To interpret the measurements we consider the flux of holes diffusing across the surface of the TiO$_2$ electrode in one dimension where the TiO$_2$ substrate is located at $x = 0$ and the outer boundary of the film is located at $x = d$. The diffusion of the holes in one dimension is described by Fick's laws according to:

$$\frac{\partial p(x,t)}{\partial t} = D_{app} \frac{\partial^2 p(x,t)}{\partial x^2} \quad \text{(A1)}$$

where p is the concentration of holes at time t and position x. For chronoabsorptometry measurements the initial condition is $p(x, t = 0) = 0$. The final condition after a step change in potential at $t = 0$ is given when all connected dye molecules on the TiO$_2$ are oxidised by holes hopping from the boundary is given by $p(x = 0, t = \infty) = p_{max}$. The boundary conditions for eqn (A1) for $t > 0$ are given by:

$$p(x = 0, t > 0) = p_{max} \quad \text{(A2)}$$

$$\frac{\partial p(x = d, t)}{\partial x} = 0 \quad \text{(A3)}$$

The solution to this equation is given by the infinite sum (see Fig. 6):

$$p(x,t) = p_{max} - \sum_{m=0}^{\infty} \frac{4p_{max}}{\pi(2m+1)} \sin\left[\frac{\pi x(2m+1)}{2d}\right]$$
$$\exp\left[-\frac{\pi^2(2m+1)^2 D_{app}}{4d^2} t\right] \quad \text{(A4)}$$
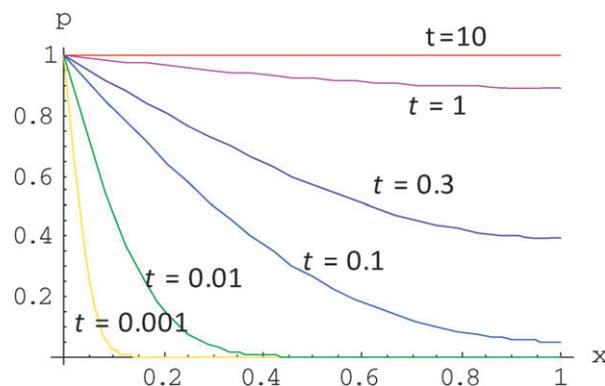
Fig. 6 Hole concentration profile (p) calculated using eqn (A4) at different times following a voltage step at $t = 0$ where $q = 1$, $p_{max} = 1$, $d = 1$, $D_{app} = 1$ and where $m = 0, 1, 2, \ldots, 100$ is used to approximate $m \to \infty$. Plots are shown at times $t = 0.001, 0.01, 0.1, 0.3, 1$ and 10.
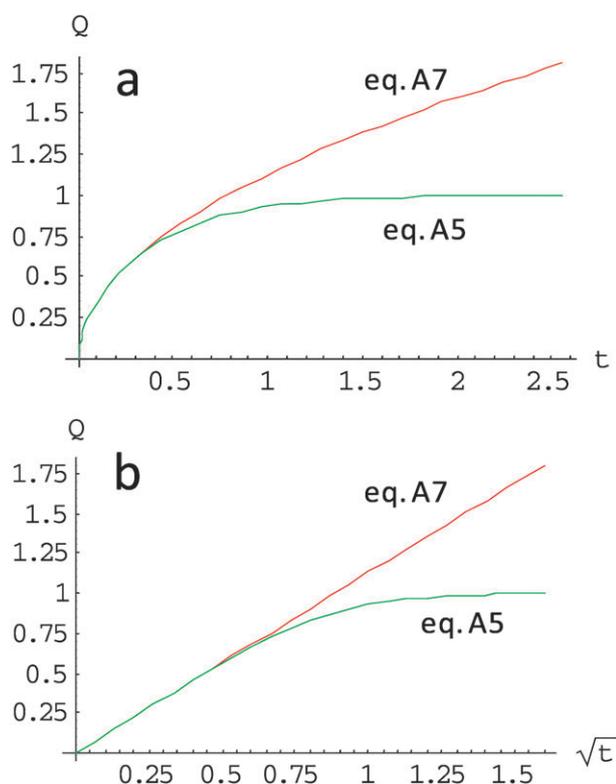
Fig. 7 The charge collected from oxidised dye molecules on TiO_2 at the substrate (Q) following a voltage step applied to the electrode at $t = 0$ using the exact solution to eqn (A1) given by eqn (A5) and the approximation given by the Cottrell eqn (A7). (a) Q plotted as a function of t. (b) Q plotted as a function of $t^{1/2}$ (an Anson plot), both curves display a linear relationship for $t^{1/2} < 0.5$. The parameters used were the same as those in Fig. 6.

The total concentration of holes in the film is given by integrating eqn (A4) with respect to x between 0 and d, so that the charge per unit area (Q) in the cell is given by:

$$Q = qp_{max}d - \sum_{m=0}^{\infty} \frac{8qp_{max}d}{(\pi + 2m\pi)}(1 + \sin[m\pi])$$

$$\exp\left[-\frac{\pi^2(2m+1)^2 D_{app}}{4d^2}\right] \quad (A5)$$

where q is the electronic charge. The dependence of Q on time is illustrated in Fig. 7.

The expression A5 can be approximated by an expression derived from the Cottrell equation at sufficiently short times. The solution to A1 with semi-infinite boundary conditions ($p(x = 0, t > 0) = p_{max}$, $p(x = \infty, t) = 0$) gives the Cottrell equation, describing the change in current density (j) at the substrate with time due the diffusion limited transfer of a species to or from the substrate following a potential step:

$$j = \frac{\partial Q}{\partial t} = 2qp_{max}\sqrt{\frac{D_{app}}{\pi t}} \quad (A6)$$

where $z = 1$ is the number of charges transferred for every hole reaching the substrate. Integrating eqn (A6) yields the amount of charge collected as a function of time:

$$Q = 2qp_{max}\sqrt{\frac{D_{app}t}{\pi}} \quad (A7)$$

Fig. 7 shows charge as a function of time calculated using eqn (A5) and (A7). It is apparent from Fig. 7 and eqn (A5) that when $t < d^2/(4D_{app})$ then Q derived using the Cottrell eqn (A7) is approximately equal to the exact solution (eqn (A5)), and a linear relationship between Q and $t^{1/2}$ is expected.

The maximum charge per unit area collected is related to p_{max} according to $Q_f = qdp_{max}$. In chronoabsorptometry, the change in absorbance (ΔOD) of the electroactive film is proportional to the charge passed (Q), thus eqn (A7) can be transformed into the corresponding eqn (4) in the main text, to derive the apparent hole diffusion coefficient D_{app}:

$$\Delta OD = \frac{2\Delta OD_f}{d}\sqrt{\frac{D_{app}t}{\pi}} \quad (A8)$$

where ΔOD_f is the change in absorbance at long times corresponding to Q_f.

Acknowledgements

Notes and references

1 B. O'Regan and M. Grätzel, *Nature*, 1991, **353**, 737.
2 E. Coronado, J. R. Galan-Mascaros, C. Marti-Gastaldo, E. Palomares, J. R. Durrant, R. Vilar, M. Gratzel and M. K. Nazeeruddin, *J. Am. Chem. Soc.*, 2005, **127**, 12351–12356.
3 Y. Astuti, E. Topoglidis, G. Gilardi and J. R. Durrant, *Bioelectrochemistry*, 2004, **63**, 55–59.
4 A. A. Mills and M. S. Lee, *J. Photochem. Photobiol., A*, 2002, **152**, 233–247.
5 X. Li, A. N. M. Green, S. Haque, A. Mills and J. R. Durrant, *J. Photochem. Photobiol., A*, 2004, **162**, 253–259.
6 Q. Wang, N. Evans, S. M. Zakeeruddin, I. Exnar and M. Gratzel, *J. Am. Chem. Soc.*, 2007, **129**, 3163–3167.
7 Q. Wang, S. M. Zakeeruddin, M. K. Nazeeruddin, R. Humphry-Baker and M. Gratzel, *J. Am. Chem. Soc.*, 2006, **128**, 4446–4452.
8 P. Bonhote, E. Gogniat, S. Tingry, C. Barbe, N. Vlachopoulos, F. Lenzmann, P. Comte and M. Gratzel, *J. Phys. Chem. B*, 1998, **102**, 1498–1507.
9 S. A. Trammell and T. J. Meyer, *J. Phys. Chem. B*, 1999, **103**, 104–107.
10 N. Papageorgiou, M. Gratzel, O. Enger, D. Bonifazi and F. Diederich, *J. Phys. Chem. B*, 2002, **106**, 3813–3822.
11 Q. Wang, S. M. Zakeeruddin, J. Cremer, P. Bauerle, R. Humphry-Baker and M. Gratzel, *J. Am. Chem. Soc.*, 2005, **127**, 5706–5713.
12 C. Karthikeyan, H. Wietasch and M. Thelakkat, *Adv. Mater.*, 2007, **19**, 1091–1095.
13 S. A. Haque, S. Handa, K. Peter, E. Palomares, M. Thelakkat and J. R. Durrant, *Angew. Chem., Int. Ed.*, 2005, **44**, 5740–574.
14 S. Handa, H. Wietasch, M. Thelakkat, J. R. Durrant and S. A. Haque, *Chem. Commun.*, 2007, 1725–1727.
15 A. Morandeira, *et al.*, *Chem. Commun.*, submitted.

16 A. Hagfeldt and M. Gratzel, *Chem. Rev.*, 1995, **95**, 49–68.
17 E. Laviron, *J. Electroanal. Chem.*, 1979, **101**, 19–28.
18 E. E. Bancroft, J. S. Sidwell and H. N. Blount, *Anal. Chem.*, 1981, **53**, 1390–1394.
19 J. B. He, Y. Wang, N. Deng, Z. G. Zha and X. Q. Lin, *Electrochim. Acta*, 2007, **52**, 6665–6672.
20 A. A. Nekrasov, V. E. Ivanov, O. L. Gribkova and Vannikov, *Electrochim. Acta*, 2005, **50**, 1605–1613.
21 A. A. Nekrasov, V. F. Ivanov and A. V. Vannikov, *Electrochim. Acta*, 2001, **46**, 3301–3307.
22 L. M. Huang, T. C. Wen and A. Gopalan, *Electrochim. Acta*, 2006, **51**, 3469–3476.
23 A. Szkurlat, B. Palys, J. Mieczkowski and M. Skompska, *Electrochim. Acta*, 2003, **48**, 3665–3676.
24 N. Gimeno, X. Li, J. R. Durrant and R. Vilar, *Chem.–Eur. J.*, 2008, **14**, 3006–3012.
25 A. J. Bard and L. R. Faulkner, *Electrochemical Methods: Fundamentals and Applications*, John Wiley & Sons, 2nd edn, 2001.
26 M. K. Nazeeruddin, R. Humphry-Baker, P. Liska and M. Grätzel, *J. Phys. Chem. B*, 2003, **107**, 8981–8987.
27 M. K. Nazeeruddin, D. Di Censo, R. Humphry-Baker and M. Gratzel, *Adv. Funct. Mater.*, 2006, **16**, 189–194.
28 P. Atkins and J. De Paula, *Physical Chemistry*, Oxford University Press, Oxford, UK, 7th edn, 2002.
29 Y. Astuti, *Bio-Functionalised Nanostructured Metal Oxide Electrodes*, PhD thesis, Imperial College, London, 2005.
30 J. E. Moser, D. Noukakis, U. Bach, Y. Tachibana, D. Klug, J. R. Durrant, R. Baker and M. Gratzel, *J. Phys. Chem. B*, 1998, **18**, 3649–3650.
31 H. Zabri, I. Gillaizeau, C. Bignozzi, S. Caramori, M. Charlot, J. Cano-Boquera and F. Odobel, *Inorg. Chem.*, 2003, **42**, 6655–6666.
32 W. H. Leng, P. R. F. Barnes, M. Juozapavicius, B. C. O'Regan and J. R. Durrant, *J. Phys. Chem. Lett.*, 2010, **1**, 967–972.
33 M. Sahimi, *Application of Percolation Theory*, Taylor & Francis, 1994.
34 E. Palomares, R. Vilar and J. R. Durrant, *Chem. Commun.*, 2004, 362–363.
35 A. Y. Anderson, P. R. F. Barnes, J. R. Durrant and B. C. O'Regan, *J. Phys. Chem. C*, submitted.
36 J. E. Kroeze, N. Hirata, S. Koops, M. K. Nazeeruddin, L. Schmidt-Mende, M. Grätzel and J. R. Durrant, *J. Am. Chem. Soc.*, 2006, **128**, 16376–16383.